Adsorption of commercial glyphosate by MOF-808: a new ZrMOF for water purification

Caroline B. C. Almeida[1] · Célia M. Ronconi[2] · Danilo R. H. de Miranda[2] · Isabela A. A. Bessa[2] · Honório C. de Jesus[3] · Priscilla P. Luz[1]

Abstract

This work reports for the first time the use of MOF-808 for the adsorption of glyphosate from a diluted herbicide formulation (Roundup®). MOF-808 was synthesized in organic solvent (MOF-808(DMF)) or in water (MOF-808(H_2O)) to compare the influence of textural characteristics on the adsorption process. In addition, the adsorption performances of these materials were compared to those of the UiO-66 and UiO-66(NH_2) series materials, which have the same SBU, allowing us to evaluate the influence of the topicity and functionalization of the ligand on the adsorption capacity of glyphosate. MOF-808 showed the highest adsorption capacity, reaching a q_{max} equal to 277.01 mg g^{-1}, and good kinetic performance, removing 70.3% of the glyphosate from solution in 10 min and 99.5% after 3 h of contact. MOFs UiO-66 and UiO-66(NH_2) had lower q_{max} values than MOF-808, possibly due to the blockage of their narrow pores by GLY, which prevents them from accessing Zr sites. The results showed an important relationship between the hydrodynamic diameter and the pore size distribution with access to active sites, consequently influencing the adsorption performance of these porous materials.

Keywords MOF-808 · UiO-66 · ZrMOF · Glyphosate · Roundup®

1 Introduction

The use of pesticides to improve efficiency and reduce costs in crop production has been growing alongside the demand for food [33]. The herbicide currently most consumed worldwide is glyphosate (GLY, N-(phosphonomethyl)glycine) [41]. This organophosphate is a nonselective systemic herbicide with a broad spectrum of activity and is a phosphonate amino acid derived from glycine that contains phosphonate (–PO(OH)$_2$), carboxylate (–CO$_2$H) and amino (–NH) groups [4, 11, 51].

The active compound of the Roundup® commercial formulation GLY was introduced to the market by the Monsanto Company in 1974 for the control of weeds in agricultural fields [34]. After being administered in plantations and leached into the soil by the action of rainwater, GLY can be biodegraded, immobilized in minerals, become biologically inactive, or reach groundwater and tributaries [50], where its half-life will depend on several factors, such as soil conditions and temperature [41].

Given the harm to human health resulting from exposure to this herbicide [3, 10, 46], several strategies have been developed for water decontamination, including photodegradation [49], membrane filtration [26], biodegradation [22], advanced oxidative processes and adsorption [26], which is one of the most studied and viable techniques for this purpose [24]. Among the adsorbent materials with the best performance in GLY adsorption are metal-organic frameworks (MOFs), which have emerged as promising materials for this application [14, 21, 23, 38, 42, 57].

MOFs are coordination polymers of the type coordination networks [6] with high crystallinity and permanent porosity

✉ Priscilla P. Luz
priscilla.luz@ufes.br

Caroline B. C. Almeida
carolbatistin_@hotmail.com

[1] Postgraduate Program in Chemistry, Inorganic Chemistry Laboratory, Federal University of Espírito Santo, Espírito Santo 29075-910, Brazil

[2] Laboratory of Nanotechnology and Supramolecular Chemistry, Department of Inorganic Chemistry, Federal Fluminense University, Rio de Janeiro 24220-900, Brazil

[3] Postgraduate Program in Chemistry, Analytical Chemistry Laboratory, Federal University of Espírito Santo, Espírito Santo 29075-910, Brazil

[13], even after removal of guest molecules from their pores as synthesis solvents [19]. The possibility of modifying the textural characteristics of these materials, such as changes in pore size and chemical environment, makes them interesting for applications in gas storage, drug delivery, membranes, sensors, catalysts, and mainly processes involving adsorption [15, 29].

Some of these properties make MOFs promising adsorption materials. The main advantage arises from the high availability of active sites (in the inorganic units or in the ligands), which can be accessed, even inside the particles, through the pores of the material, whose size can be regulated by the length and/or topicity of the chosen ligand or by network defect induction techniques (hierarchical MOF) [17, 27, 44, 56]. It is also possible to use functionalized ligands [9, 17] or to perform postsynthetic functionalization, maintaining the crystalline network, generating intraporous active sites, and adapting to the chemical characteristics of the adsorbate [5, 35].

Since 2015, dozens of networks have been evaluated for GLY adsorption in aqueous environments. Zhu et al. [57] were the pioneers in this application of the UiO-67 MOF based on the use of zirconium knots (ZrMOF) and a GLY adsorption capacity equal to 537 mg g^{-1}, a value that surpassed that of zeolites, mesoporous silicas, biochar, graphene and other reported non-MOF materials at that time [39]. In the following years, the NU-1000 MOF, containing the same UiO-67 secondary building units (SBUs) but using a long-chain tetradentate ligand, reached a capacity of 1516 mg g^{-1}, a value still not surpassed by that of other materials [38]. Studies of MOFs functionalized with short carboxylate ligands, functionalized or not, with the metals chromium ((NH$_2$)MIL-101(Cr)), iron (MIL-101(Fe)) and titanium (MIL-125-Ti) have also been reported, reaching maximum values of 440 mg g^{-1} [17, 30, 36].

Among the best performing MOFs, ZrMOFs already reported have an SBU containing a Zr$_6$ cluster that strongly interacts with the phosphonate group of GLY, acting as a Lewis acid center [16, 38, 57]. The affinity between these groups increases with the number of Zr-OH-Zr bonds in the SBU and with the induction of defects due to the missing ligand coordinated to the cluster [38, 57].

In this work, we report for the first time the use of MOF-808 for the adsorption of GLY from a diluted commercial herbicide formulation (Roundup®), bringing the results closer to real application. MOF-808 contains the same Zr$_6$ cluster as do UiO-67 and NU-1000 MOFs, but its six ligands (trimesic acid and tritopic) coordinate to the SBU, leading to a s*pn* network topology with a reported pore diameter of approximately 18 Å. In addition, MOF-808 was synthesized by two experimental routes (in organic solvent and water) to evaluate the adsorption capabilities of the same MOF with different textural characteristics.

We also compared these results with those of the UiO-66 series, where the topicity of the ligand (terephthalic acid – ditopic) was reduced, changing the network topology (*fcu*) and the access of the adsorbate to the active sites. Finally, we investigated whether the use of an amino-functionalized ligand would increase the efficiency of adsorption.

The pseudo-first order, pseudo-second order and Weber–Morris models were applied to the adsorption kinetics results. We also fit the Langmuir and Freundlich models to the adsorption isotherms to determine the equilibrium involved in this process.

2 Experimental

2.1 Materials

The reagents used were used as received. Zirconium chloride IV (ZrCl$_4$, ≥ 98%), trimesic acid (H$_3$BTC, ≥ 95%), 2-aminoterephthalic acid (H$_2$BDC-NH$_2$, ≥ 99%), terephthalic acid (H$_2$BDC, ≥ 98%), hydrochloric acid (HCl, 37%) and acetone (PA) were obtained from Sigma−Aldrich Co. N–N-dimethylformamide ((CH$_3$)$_2$NCH, ≥ 99.8%) and absolute ethanol (C$_2$H$_6$O, ≥ 99.5%) were obtained from Dinâmica Química Contemporânea LTDA. Methanol (CH$_3$OH, ≥ 99.8%) and acetic acid (CH$_3$COOH, ≥ 99.5%) were obtained from Neon Comercial Reagentes Analíticos LTDA. Chloroform (CHCl$_3$, ≥ 99.8%) was obtained from Vetec Química Fina Ltda. The Roundup® commercial glyphosate (N-(phosphonomethyl)glycine, 480 g/L) was purchased from Monsanto do Brasil LTDA.

2.2 Synthesis of ZrMOFs

2.2.1 MOF-808(DMF)

MOF-808(DMF) was synthesized following the methodology described by Xu et al. [52]. ZrCl$_4$ (1.05 g, 4.5 mmol) was dissolved in 45 mL of acetic acid, and H$_3$BTC (0.31 g, 1.5 mmol) was dissolved in 45 mL of DMF under sonication for 30 min. These solutions were mixed and kept under an ultrasound bath for another 30 min, and the obtained solution was transferred to a high-pressure reactor lined with Teflon and kept at 120 °C for 72 h. The obtained white solid was washed with acetone four times and dried at 100 °C for 12 h, followed by activation in CHCl$_3$ at 50 °C for three days, with chloroform renewed once a day. Finally, activation was performed by heating at 120 °C for 24 h under vacuum.

2.2.2 MOF-808(H$_2$O)

MOF-808(H$_2$O) was synthesized following the procedure described by Liu et al. [31]. H$_3$BTC (210 mg, 1.0 mmol), acetic acid (10 mL), deionized water (10 mL), ZrCl$_4$ (700 mg, 3.0 mmol) and concentrated HCl (100 μL) were added to a round bottom. The mixture was stirred and heated at 110 °C for 18 h. The resulting white solid was separated by centrifugation and washed in distilled water for one day under stirring at room temperature, after which the water was changed once a day. Then, the MOF was suspended in 1 mol/L HCl and stirred for 12 h at 90 °C. Finally, the MOF was separated by centrifugation, washed three times in water, three times in absolute ethanol and dried under vacuum at 120 °C for 24 h.

2.2.3 UiO-66

UiO-66 was synthesized using a method adapted from Cavka et al. [8]. ZrCl$_4$ (0.053 g, 0.227 mmol) and H$_2$BDC (0.034 g, 0.227 mmol) were dissolved in DMF (24.9 g, 340 mmol) at room temperature in an ultrasound bath. The obtained solution was transferred to a Teflon-lined high-pressure reactor at 120 °C for 24 h. The product was washed with DMF three times and centrifuged. MOF activation was performed in methanol for 24 h under stirring at room temperature, followed by centrifugation and activation at 120 °C for 24 h under vacuum.

2.2.4 UiO-66(NH$_2$)

UiO-66(NH$_2$) was synthesized following the procedure adapted from Chavan et al. [9]. ZrCl$_4$ (0.3956 g, 0.227 mmol) and H$_2$BDC-NH$_2$ (0.3074 g, 0.227 mmol) were dissolved in 46 mL of DMF (24.9 g, 340 mmol) and 39 μL of deionized water in an ultrasound bath. Then, the solutions were mixed and kept under ultrasound for 10 min and transferred to a high-pressure reactor lined with Teflon at 100 °C for 72 h. The resulting white solid was separated by centrifugation and washed three times in DMF (40 mL), followed by solvent exchange in water under stirring for 2 h at 85 °C. Finally, the solid was dried at 60 °C for 24 h under vacuum.

2.3 Glyphosate adsorption tests

For commercial glyphosate adsorption tests, a 0.1 mol/L stock solution was prepared by dissolving 3.48 mL of Roundup® in 100 mL of distilled water. This stock solution was diluted from 0.025 to 1.0 mmol/L, and the resulting solutions were subjected to adsorption tests. The kinetic properties of the adsorption process were investigated from the residual concentration of GLY in solution. For this purpose, the residual phosphorus content was determined via inductively coupled plasma−optical emission spectrometry (ICP−OES), and its concentration was associated with the glyphosate concentration. All tests were performed in triplicate.

2.3.1 Kinetic tests

The GLY adsorption kinetics were evaluated by adding 5 mg of each MOF to 25 mL of a 0.1 mmol/L GLY solution. The samples were agitated on a shaking table at 180 rpm and 22 °C for specific durations, ranging from 10 min to 5 h. The MOFs were removed from the solutions by centrifugation after each test. The adsorbent mass ratio was 0.2 g/L of solution. The adsorption capacity of GLY on the MOFs at each time was calculated from Eq. 1:

$$q_t = (C_0 - C_t)V/W \tag{1}$$

where q_t is the adsorbed amount (mmol g^{-1}); C_0 and C_t correspond to GLY concentrations (mmol L^{-1}) at initial time and time t(min), respectively; V is the volume (L) of GLY solution used; and W is the mass (g) of adsorbent used [57].

2.3.2 Adsorption equilibrium

For the adsorption equilibrium test, 25 mL of GLY solution at different concentrations (0.025 to 1.0 mmol L^{-1}) were stirred with 5 mg of each MOF for 4 h at 22 °C and 180 rpm.

2.3.3 Data analysis of GLY adsorption tests

The kinetic adsorption properties of the materials were investigated. The results were adjusted to pseudo-first order, pseudo-second order and Weber and Morris intraparticle diffusion models by linearized Eqs. 2 to 4, respectively:

$$ln(q_e - q_t) = lnq_e - k_1t \tag{2}$$

$$t/q_t = 1/k_2q_e^2 + t/q_e \tag{3}$$

$$q_t = K_d t^{0,5} + I \tag{4}$$

q_e and q_t (mg g^{-1}) are the amounts of GLY adsorbed by ZrMOF at equilibrium and at time (t), respectively; k_1 is the PFO adsorption rate constant (min^{-1}); k_2 is the PSO adsorption rate constant (g mg^{-1} min^{-1}); K_d is the intraparticle diffusion coefficient (g mg^{-1} min$^{-0.5}$); and I is the linear intercept related to diffusion resistance (mg g^{-1}) [2].

The adsorption equilibrium data were fitted to the Langmuir and Freundlich models using the respective linearized equations (Eqs. 5 and 6), where

$$C_e/q_e = 1/q_{max}K_L + C_e/q_{max} \qquad (5)$$

$$log\,q_e = \frac{1}{n}log\,C_e + log\,K_F \qquad (6)$$

C_e(mg/L) is the GLY concentration at equilibrium, q_{max} (mg/g) is the maximum adsorption capacity needed to reach the K_L constant; related to the availability of binding sites with GLY in the Langmuir model, K_F is the representative constant of the adsorption capacity coefficient, and *n is* the adsorption intensity in the Freundlich model [43, 47].

2.4 Instrumentation

The degree of material crystallization was evaluated via X-ray powder diffraction (PXRD) analysis at room temperature with a Shimadzu model XRD-6000 diffractometer with Cu-K$_\alpha$ radiation ($\lambda = 1.5418$ Å), and the diffraction angle (2θ) varied from 5 to 50° in 0.01° intervals at a voltage of 40 kV and current of 30 mA. Thermogravimetric analysis (TGA) and differential thermal analysis (DTA) were carried out in a Shimadzu TM TA-60WS apparatus under an inert atmosphere at a heating rate of 10 °C min^{-1} and a gas flow rate of 100 mL min^{-1} to a maximum temperature of 900 °C in Al$_2$O$_3$ crucibles. Scanning electron microscopy (SEM) and energy dispersive X-ray spectroscopy (EDS) were performed using a JSM-6610 microscope. Transmission electron microscopy (TEM) was performed using a Jeol-JEM 1400 apparatus (Japan) at 120 kV. N$_2$ adsorption and desorption isotherms were obtained at -196 °C with an ASAP 2020 V304 e-serial 1200 instrument. Specific surface areas were calculated using the Brunauer–Emmett–Teller (BET) equation. The cumulative pore volumes and pore size distributions were obtained using the nonlocal density functional theory (NLDFT) method. Dynamic light scattering (DLS), and zero charge potential (p$_{cz}$) analyses were performed using the Zetasizer advance Lab Blue (Malvern) instrument equipped with a blue laser ($\lambda = 466$ nm) and a detection angle of $\theta = 90°$ at 25 °C. The quantification of glyphosate

was performed by determining phosphorus through the ICP−OES technique using a Perkin-Elmer Optima 3000 spectrometer in axial view mode and with a phosphorus emission line at 213.617 nm. The plasma was operated at 1300 W, with an argon flow (L min^{-1}) of 15 for the plasma gas, 0.2 for the auxiliary gas and 0.8 for the nebulizer.

3 Results and discussion

3.1 Characterization of ZrMOFs

The PXRD patterns obtained for the synthesized ZrMOFs are shown in Fig. 1. All the samples had high crystallinity and peaks corresponding to the 1,002,672 (MOF-808) and 733,458 (UiO series) standards indexed at the Cambridge Crystallographic Data Center, confirming the reproduction of the compounds.

The TGA for the ZrMOFs revealed three important mass loss events (Fig. 2). The first stage is evidenced by the endothermic peak in the DTA curve at approximately 100 °C, corresponding to the loss of intrapore water, which is physiosorbed in the ZrMOF channels. A large mass loss corresponding to water is expected for MOF-808, which is known to be highly hygroscopic [20].

The second mass loss event corresponds to the removal of solvents trapped inside the pores or coordinated to the SBUs and to the dehydroxylation of the zirconium oxoclusters [1, 45]. This step occurs during heating in the region between the dehydration of ZrMOFs and their thermal decomposition. MOF-808 and UiO-66(NH$_2$) have a considerable amount of solvent in the network, approximately 17% by mass (Table 1). The third mass loss corresponds to the breaking of bonds between the benzene ring of the ligand and the SBU, the decomposition of the ligand into CO and CO$_2$, the formation of ZrO$_2$ and the consequent loss of the crystalline network [40]. Since there are no well-defined plateaus separating the second from the third event, it is inferred that they occur simultaneously as

Fig. 1 PDRX patterns of (**a**) MOF-808 synthesized in DMF and in water and (**b**) UiO-66 and UiO-66(NH$_2$) compared to the corresponding patterns indexed at the Cambridge Crystallographic Data Centre
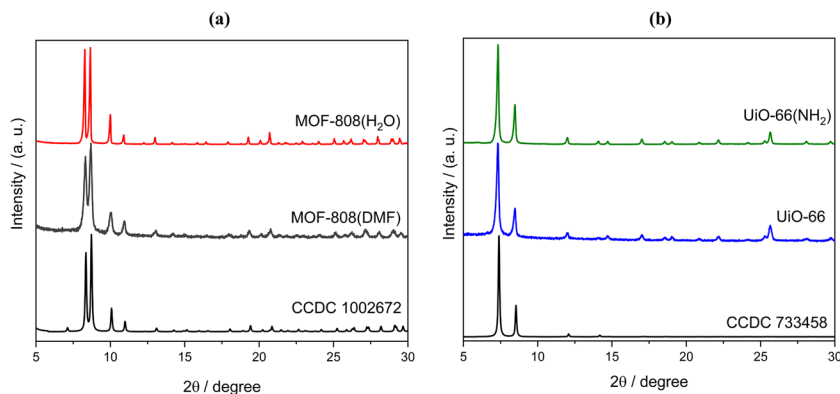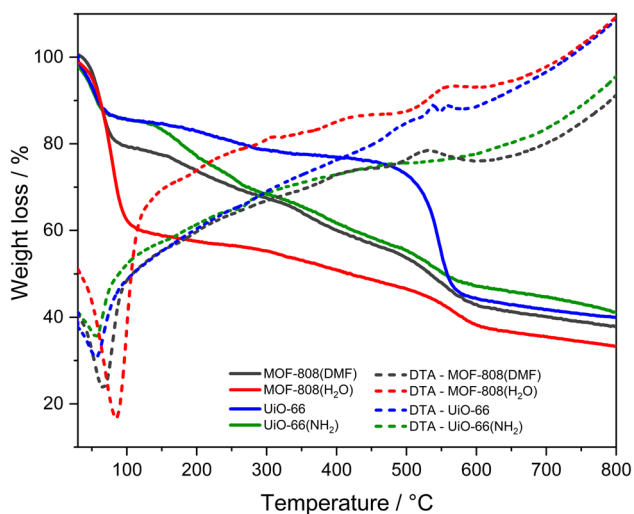
Fig. 2 TGA (continuous line) and DTA (dotted line) results for ZrMOFs

the sample is heated; therefore, the network starts decomposing during the removal of the auxiliary ligand (solvent and/or modulator) [9]. The exothermic peaks of DTA at approximately 550 °C indicate alteration of the crystalline phase of the material, which is expected due to the decomposition of the crystalline network with subsequent formation of ZrO_2, which is the residue [9]. In the case of UiO-66(NH$_2$), the DTA curve does not show ligand decomposition due to the thermolability of aminoterephthalic acid, which gradually decomposes in the MOF network at relatively low temperatures compared to UiO-66. Therefore, we estimated that the decomposition temperature was 300 °C, as reported in the literature [18]. After the third event, no plateau is achieved in the formation of residual ZrO_2 for all the ZrMOFs [9, 31, 52]. The temperature and mass percentage attributed to each thermal event are listed in Table 1.

The synthesized ZrMOF exhibited high thermal stability, maintaining its crystalline network up to approximately 400 °C, except for UiO-66(NH$_2$), which was stable up to 300 °C. These values are slightly lower than those reported in previous works, possibly due to structural defects [18]. To investigate the presence of these defects in ZrMOFs by TGA, the observed molar ratios between the metal and ligand were compared to the expected values already reported. Table 2 presents the molar ratios observed in the thermogravimetric data, as previously reported by Reinsch et al. [40], and compared to the theoretical values for each MOF. The metal content was estimated by the residue formed at 900 °C and the linker by the mass loss in the third thermal event. All ZrMOFs exhibit some degree of ligand-based defects, which are expected for those synthesized in acetic acid,these defects act as modulators by coordinating with the SBU and preventing network growth [31]. The presence of defects leads to larger pores than in the respective ideal structure [16, 18].

The ZrMOF morphology observed by SEM (Fig. 3) was not well defined, as particles, except for MOF-808(H$_2$O), were highly aggregated and spherical in shape. From the TEM images, edges and vertices of crystals of the MOF-808(DMF) and UiO-66 series can be observed, indicating the formation of octahedral crystals [28, 42, 52]. Furthermore, MOF-808(H$_2$O) exhibited the largest particles.

N$_2$ adsorption/desorption isotherms, cumulative pore volumes and pore size distributions are shown in Fig. 4. All the analyzed materials exhibited type I isotherms according to the International Union for Pure and Applied Chemistry (IUPAC) classification (Fig. 4a) [53]. This profile is characterized by significant N$_2$ adsorption at low relative pressures (w/p$_0$ < 0.05) due to the strong adsorbent-adsorbate interactions in the micropores of these materials. MOF-808(H$_2$O) showed two micropore distributions (Fig. 4b), with the smallest pore sizes between 1.0 nm and 1.3 nm and the second largest distribution with micropore sizes between 1.4 nm
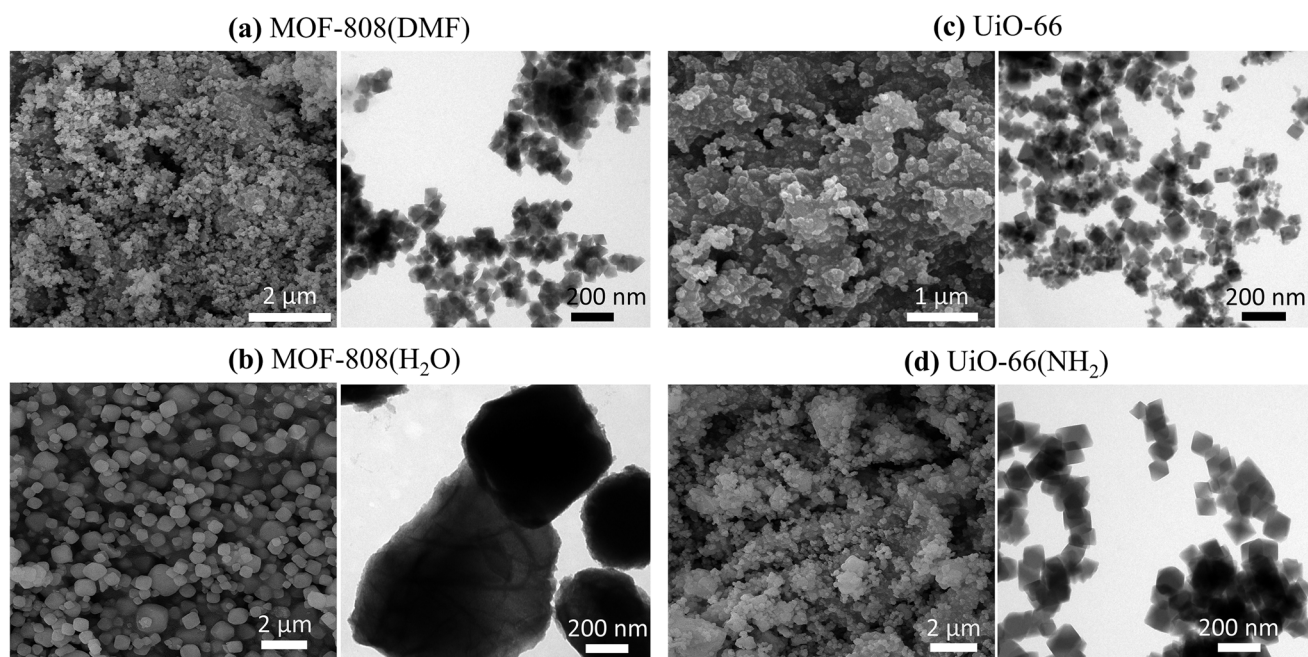
Table 1 The temperature range (approximately) and percentage of thermal mass loss are presented in the TG analysis of MOF-808(DMF), MOF-808(H$_2$O), UiO-66 and UiO-66(NH$_2$)

MOF	1st event		2nd event		3rd event	
	T (°C)	Weight loss (%)	T (°C)	Weight loss (%)	T (°C)	Weight loss (%)
MOF-808(DMF)	up to 95	20.4	95—380	17.8	380—630	20.2
MOF-808(H$_2$O)	up to 130	40.3	130—450	10.8	450—650	12.4
UiO-66	up to 95	14.8	95—435	8.11	435–611	33.1
UiO-66(NH$_2$)	up to 90	14.1	90—300	16.8	300—610	21.9

Table 2 Expected and observed molar ratios of Zr/linker deduced from thermogravimetric experiments

MOF	MOF-808(DMF)	MOF-808(H$_2$O)	UiO-66	UiO-66(NH$_2$)
Expected reason[49]	6:2	6:2	1:1	1:1
Observed reason	6:1.9	6:1.4	1:0.7	1:0.4
Thermal stability (°C)	380	450	435	300

(a) MOF-808(DMF)

(c) UiO-66

(b) MOF-808(H$_2$O)

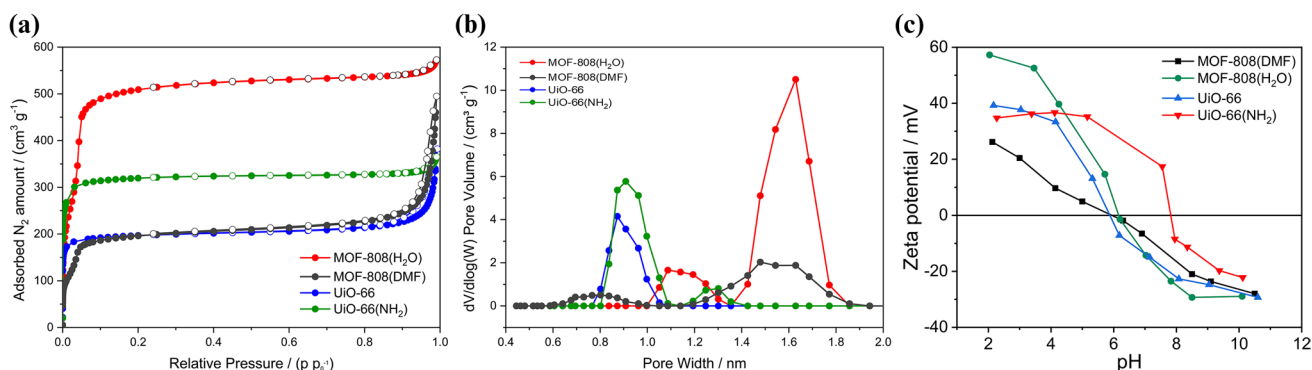**(d)** UiO-66(NH$_2$)

Fig. 3 SEM (left) and TEM (right) images of the ZrMOFs

Fig. 4 **a** Nitrogen adsorption and desorption isotherms obtained at -196 °C, **b** pore size distribution obtained by NLDFT and (**c**) variation in the zeta potential as a function of pH for ZrMOFs

and 1.9 nm. This profile causes two changes in the inclination of the isotherm at low pressure (Fig. 4a), indicating saturation of the narrowest pores followed by the widest pores. An analogous profile was observed for MOF-808(DMF), but the pore size distributions ranged from 0.8 nm to 1.1 nm and from 1.2 nm to 1.9 nm. The greater amount of larger pores observed for MOF-808(H$_2$O) compared to MOF-808(DMF) and for UiO-66(NH$_2$) compared to UiO-66 may be related to the presence of defects (absence of ligand), as indicated in Table 2 [42].

The isotherms of UiO-66 and MOF-808(DMF) show a significant increase in N$_2$ adsorption at relative pressures close to 1 (Fig. 4a), which is common in materials whose

particles are agglomerated, as observed in the SEM images of these MOFs. In summary, Table 3 presents the textural characterization data of the ZrMOFs, their specific surface area (S$_{BET}$), and total pore volume.

The BET area of MOF-808(H$_2$O) is larger than that of MOF-808(DMF), possibly due to the synthesis and activation methods used, ensuring the formation of defects, and unclogging of the MOF pores during solvent removal, as also shown by the TGA data. The formation of defects in the UiO-66(NH$_2$) network was caused by the thermolysis of the ligand during purging before N$_2$ adsorption analysis, possibly giving this MOF a larger BET area than UiO-66 [18].

Table 3 Specific surface area (S_{BET}) and total pore volume of the materials. Hydrodynamic diameter measured in water and PdI values

| MOF	S_{BET} (m^2 g^{-1})	V_{total} (cm^3 g^{-1})	Hydro-dynamic diameter (nm)	PdI
MOF-808(DMF)	725.70	0.646	277.0	0.395
MOF-808(H$_2$O)	1990.08	0.786	596.5	0.588
UiO-66	766.56	0.509	439.4	0.483
UiO-66(NH$_2$)	1248.31	0.519	480.4	0.537

The hydrodynamic diameter of the MOFs in water and the polydispersity index (PdI) measured by dynamic light scattering are also presented in Table 3. MOF-808(H$_2$O) exhibited the largest particle size obtained by hydrodynamic diameter, and MOF-808(DMF) had the smallest particle size. ZrMOFs exhibit an intermediate polydispersity index, and some reported works correlate MOF particle size with dispersion stability [12, 32]. MOFs with larger particle sizes tend to have lower hydrodynamic stability and consequently higher PdI. These data corroborate the SEM images where MOF-808(H$_2$O) has a larger particle size than the other ZrMOFs.

The potentiometric titration curves as a function of pH (Fig. 4c) show an isoelectric point close to pH 6 for the MOF-808(DMF), UiO-66 and UiO-66(NH$_2$) samples. In the range of pH 5.9–6.2, the three samples have practically neutral surface charges. However, MOF-808(H$_2$O) has an isoelectric point at pH ~ 8 and a positive surface charge at lower pH values.

3.2 Adsorption of GLY by ZrMOFs

3.2.1 Adsorption kinetics

Glyphosate has a zwitterionic nature. At the pH of the adsorption tests (below 5.8), it is in its anionic forms (GLY$^-$ and GLY^{2-}) thus, electrostatic interactions with the positive surface of ZrMOFs favor the adsorption process [16]. Confirming what was expected, the ZrMOFs showed excellent Roundup® removal capabilities from the aqueous system analyzed. The percentage of residual GLY in the solutions was reduced by approximately 70% after just 10 min of contact with MOF-808 (DMF) in combination with the diluted Roundup® herbicide solution, reaching 99.5% after 5 h (Fig. 5). Although MOF-808(H$_2$O) has the same crystal lattice, it is kinetically slower at removing GLY; it removes 70.3% of the GLY after only 60 min of contact, but it statistically achieves the same performance at equilibrium. The UiO-66 series
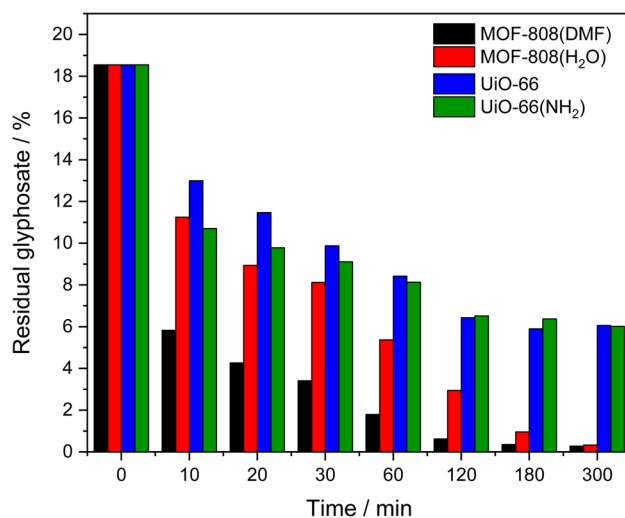
Fig. 5 Percentage of residual glyphosate in test solutions after adsorption by ZrMOFs at contact times ranging from 10 to 300 min

achieved a 68% reduction in GLY concentration after 5 h of contact.

The adsorption isotherms show the adsorption capacities (q_t) obtained as a function of time (Fig. 6a). MOF-808(DMF) reaches 69.3% of its q_t in 10 min and 82.8% in 30 min. As the adsorption process is a surface phenomenon, the number of sites exposed to the adsorbate is one of the main factors that accelerates adsorption [30]. Since adsorbent-adsorbate contact initially occurs on the external surface of a material, the smaller the MOF particle size is, the greater the number of external sites exposed to the adsorbate [47]. Pankajakshan et al. [38] reported that the particle size of ZrMOFs was inversely proportional to the adsorption capacity of GLY when investigating particles ranging from 100 to 2000 nm. Given the smaller hydrodynamic diameter of MOF-808(DMF) in water compared to that of other ZrMOFs, the excellent kinetic performance of MOF-808(DMF) is justified by the greater number of exposed external sites when the material is dispersed in aqueous media [38, 57].

UiO-66 and UiO-66(NH$_2$) showed almost the same performance overall (Fig. 6a), with amino functional groups reaching higher adsorption percentages after up to 30 min. Possibly, this better performance was associated with the greater number of pores with a larger diameter (1.3 nm), which facilitates internal diffusion since they have approximately the same hydrodynamic diameters. The presence of the amino group did not influence the adsorption capacity of the UiO-66 series, indicating that GLY-MOF interactions do not occur via interactions with this group. Notably, in this work, the pH was not regulated during the adsorption tests because we used GLY from the dilution of the commercial herbicide Roundup®, bringing the test conditions closer to
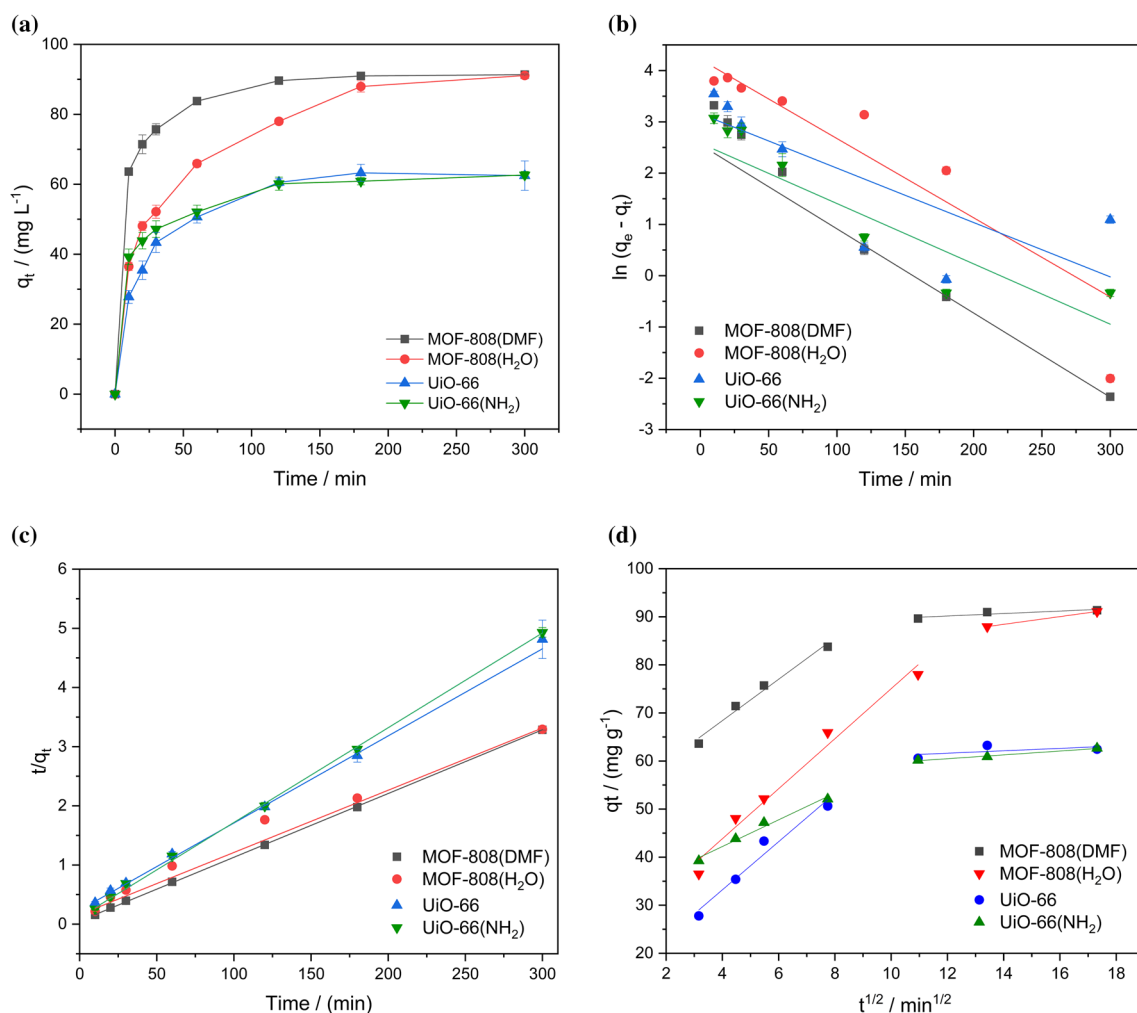
Fig. 6 **a** Glyphosate adsorption capacity as a function of contact time with ZrMOFs. The initial glyphosate concentration was 0.1 mmol/L, the pH was 5.6–5.8, and the temperature was 22 °C. **b** Pseudo-first order model, **c** Pseudo-second order model and (**d**) intraparticle diffusion model

conditions close to those of agricultural application. Therefore, the amino group did not influence the adsorption capacity of UiO-66(NH2) to the detriment of UiO-66 under the test conditions. Other studies achieved better performance using functionalized ligands but under strongly acidic pH conditions [17].

As the adsorption sites are occupied, the MOF pores become obstructed, the adsorption rate decreases, and adsorption equilibrium is reached. For MOF-808(DMF), UiO-66 and UiO-66(NH$_2$), equilibrium is reached within 2 h, and for MOF-808(H$_2$O), equilibrium is reached within 3 h, possibly due to the intrapore larger active sites, since internal diffusion is slower than adsorption on the external surface, as observed for MOF-808(DMF), UiO-66 and UiO-66(NH$_2$).

Adsorption kinetics provide important information about process speed, adsorbent performance and mass transfer mechanisms [47]. The pseudo-first order, pseudo-second

order and Weber–Morris intraparticle diffusion models were applied to the isotherm data, and the results are shown in Fig. 6b–d, respectively; their respective kinetic parameters are listed in Table 4. In all the cases, the PSO model better fits the experimental results, both by analyzing the coefficient of determination and by the values of q$_e$ calculated by the model associated with the values obtained experimentally. The PSO model indicates that ZrMOFs have an abundant number of adsorption sites, with chemisorption being the determining step in the rate of adsorption of GLY [16, 37].

The Weber−Moris intraparticle diffusion plots (Fig. 6d) show two stages for the adsorption of GLY on ZrMOFs, represented by two linear segments. The first stage is attributed, as previously reported, to diffusion in the boundary layer where GLY is transferred from the solution (external mass) to the surface of the ZrMOFs [57]. The second stage is attributed to the internal diffusion of GLY through the pores

Table 4 Kinetic parameters for the adsorption of glyphosate on ZrMOFs

MOF	Pseudo-first order model			Pseudo-second order model			Intraparticle diffusion model		
	k_1 (L mol^{-1})	q_e (mg g^{-1})	R^2	k_2 (min^{-1})	q_e (mg g^{-1})	R^2	K_i	I (mg g^{-1})	R^2
MOF-808(DMF)	0.016	12.88 ± 1.10	0.997	0.200	92.85 ± 4.53	0.999	0.272	86.89	0.810
MOF-808(H$_2$O)	0.015	67.96 ± 1.31	0.827	0.065	95.06 ± 5.67	0.996	0.803	77.19	0.999
UiO-66	0.011	23.52 ± 1.80	0.611	0.062	67.94 ± 3.42	0.997	0.502	55.20	0.635
UiO-66(NH$_2$)	0.012	13.25 ± 1.63	0.795	0.136	62.46 ± 4.68	0.998	0.386	55.79	0.973

of the ZrMOFs. According to the WB model, the intersection of the segments with the origin of the graph indicates that the process rate is exclusively controlled by the intraparticle diffusion step, which does not occur during the adsorption of GLY by ZrMOFs [37]. However, MOF-808(H$_2$O) exhibited a greater inclination in the second stage than did the other ZrMOFs (Table 4), as indicated by its larger pore diameter, which allowed GLY to internally diffuse through the MOF pores. During adsorption, the pores of the other ZrMOFs are possibly obstructed, as they are narrower, hindering the internal diffusion of GLY [42].

It is worth noting that the different topologies of the ZrMOF network, arising from the different ligand topicities, generate networks with different pore sizes. Simply changing from a ditopic (BDC) to a tritopic ligand (BTC) leads to an increase in the pore aperture and diameter [53], allowing the entrance of larger guests or more molecules from the same guest. The largest dimension of the GLY molecule (8.7 Å × 4.5 Å × 4.6 Å) [56] is smaller than that of MOF-808 pores, which, in theory, allows GLY diffusion through the pores to reach the internal adsorption sites. For the UiO-66 series, adsorption possibly occurred on the outer surface of the material since the pore size of the MOF was smaller than the largest dimension of the GLY, possibly leading to pore clogging and a reduction in the adsorption rate. Tao et al. [42] reported greater adsorption capacities of GLY for UiO-66 when they synthesized

hierarchical structures (HUiO) with mesopores reaching 7.5 nm. These MOFs reached an adsorption capacity of 400 mg g^{-1} for GLY due to the increase in pore size and consequent increase in the availability of adsorption sites in the material [42].

3.2.2 Adsorption isotherms

The isotherms have an extremely favorable format for adsorption (Fig. 7a), and the mass of adsorbate retained per unit mass of adsorbent is high for a low equilibrium concentration of adsorbate in the liquid phase [39].

From the parameters obtained, as shown in Table 5, the Langmuir model better fit the experimental data (Fig. 7b) once the coefficient of determination (R^2) was higher for all the MOFs, suggesting that there was no difference in the affinity of the MOF active sites for GLY, given the homogeneity in the distribution and type of active sites predicted by the model. The K_L constant is related to the affinity of the adsorbent-adsorbate interaction, and MOF-808(DMF and H$_2$O) has a greater affinity for glyphosate than does the UiO-66 series since they exhibit the highest K_L values. Even when these ZrMOFs have the same SBUs, the pore size influences the strength of the adsorbent-adsorbate interaction. Pankajakshan et al. [38] verified by theoretical calculations that MOF NU-1000 has a greater GLY adsorption energy than UiO-67 and a smaller interatomic distance in the
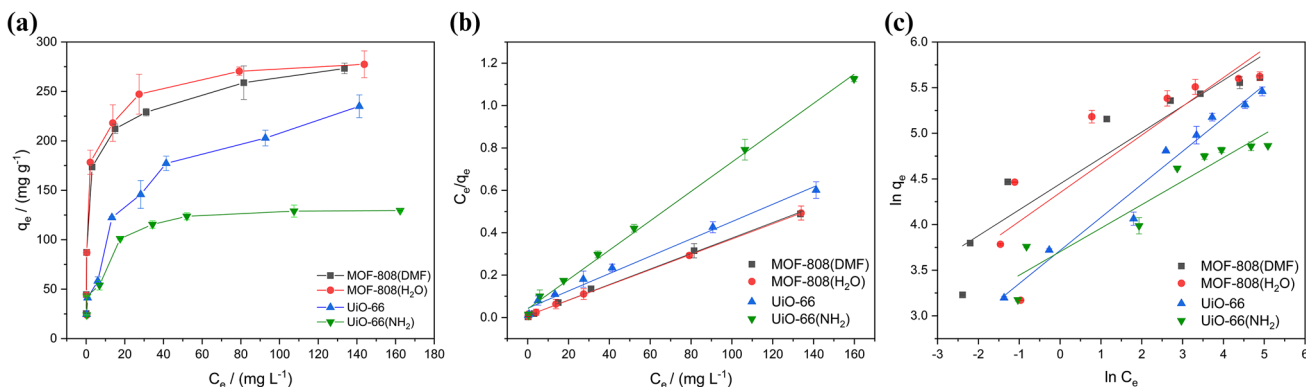

Fig. 7 Isotherms for the adsorption of glyphosate on ZrMOFs (**a**). Graphs corresponding to the (**b**) Langmuir and (**c**) Freundlich adsorption models. Adsorption conditions: 25 °C, pH 5.5, and glyphosate concentration = 0.1 mmol/L

Table 5 Parameters of the Langmuir and Freundlich models for glyphosate adsorption on ZrMOFs

MOF	Langmuir model			Freundlich Model		
	K_L (L mg^{-1})	q_{max} (mg g^{-1})	R^2	K_F (mg^{1-n} L^n g^{-1})	n	R^2
MOF-808(DMF)	0.412	273.22 ± 7.38	0.998	85.294	3.523 ± 0.023	0.880
MOF-808(H$_2$O)	0.397	277.01 ± 14.1	0.999	77.465	3.172 ± 0.014	0.758
UiO-66	0.094	244.49 ± 5.14	0.987	41.098	2.761 ± 0.038	0.970
UiO-66(NH$_2$)	0.171	144.30 ± 6.07	0.997	40.567	3.882 ± 0.029	0.905

Zr-OP bond because larger pore sizes allow greater interactions between the adsorbate and SBU [38].

The calculated q_{max} value indicated that the small BET area found for MOF-808(DMF) was compensated for by its hydrodynamic diameter, which promoted high exposure to its active sites; moreover, the larger particle size of MOF-808(H$_2$O) was compensated for by its larger BET area. The presence of large pores is important for GLY to reach active sites, and at the end of equilibrium, even with different textural characteristics, both MOF-808 exhibit approximately the same performance in removing the herbicide, regardless of the synthesis procedure adopted.

With respect to UiO-66 and UiO-66(NH$_2$), the larger BET area of UiO-66(NH$_2$) and its larger pores do not lead to higher values of q_{max}. In the adsorption of large molecules such as GLY, the specific surface area is an important factor in the adsorption capacity but is not decisive [7]. In this case, even with a larger BET area, the pores of UiO-66(NH$_2$) are as narrow as those of UiO-66, and the small number of larger pores (approximately 1.3 nm) is not enough to allow GLY access to the interior of the material. We assumed that pore obstruction occurred in both materials and that the determining factor for q_{max} was the hydrodynamic diameter, which favored UiO-66.

The q_{max} values calculated by the Langmuir model were compared with the results obtained for GLY adsorption by other MOF materials reported over the years (Table 6). Research on the application of MOFs for GLY adsorption started in 2015 with the work of Zhu et al. [57]. Since then, MOFs of different metals designed to reach mesopores have been reported for such applications.

Interestingly, although the performance of some ZrMOFs, such as NU-1000 and UiO-67, in GLY adsorption is excellent, the linkers of these MOFs are expensive, increasing the difficulty of large-scale application.[59] Approximate values of these linkers, with purities above 97%, are shown in Table 7 and were obtained in September 2023.

Even though there is variation in values due to dollar exchange fluctuations or differences in the brands of these reagents, it is notable that the NU-1000 and UiO-67 ligands are more than 320 and 30 times more expensive, respectively, than the MOF-808 ligand, which performed better in this work. MOF-808 has excellent removal capacity for commercial GLY herbicides, as determined

Table 6 Maximum glyphosate adsorption capacities calculated by the Langmuir model for the MOFs

MOF	q_{max} (mg g^{-1})	Reference
UiO-67	537.00 (298 K)	[57]
UiO-67/GO	482.69 (298 K)	[54]
(NH$_2$)MIL-101(Cr)	64.25 (298 K)	[17]
Fe$_3$O$_4$@SiO$_2$@UiO-67	256.54 (298 K)	[55]
NU-1000	1517.00 (298 K)	[38]
MIL-101(Fe)	379.98 (318 K)	[30]
NH$_2$-MIL-101(Fe)	501.46 (318 K)	[30]
UiO-66 (hierarchical MOF)	400.00 (298 K)	[42]
CuO@MIL-101(Fe)	240.20 (293 K)	[25]
UiO-67 (T2 – hierarchical)	322.58 (298 K)	[16]
NH$_2$-MIL-101@BC (NMBC$_{61}$)	186.71 (323 K)	[48][60]
MIL-125-Ti (hierarchical)	440,90 (298 K)	[36][61]
MOF-808(DMF)	273.22 (298 K)	This work
MOF-808(H$_2$O)	277.01 (298 K)	
UiO-66	244.49 (298 K)	
UiO-66(NH$_2$)	144.30 (298 K)	

by analyzing the ratio of q_{max} to the cost of synthesis. Based on these results, it is necessary to investigate the optimal conditions for the synthesis and adsorption of MOF-808 to make its application viable for the treatment of water contaminated with GLY.

4 Conclusions

The adsorption of GLY by MOF-808, which was synthesized under different synthesis conditions, was evaluated. The differences in the textural properties of MOF-808 did not reflect the maximum adsorption capacity of GLY for the material. However, a smaller particle size ensured better kinetic performance for MOF-808(DMF), which may be interesting for applications in which quick removal of organophosphate from solution is desirable. MOFs UiO-66 and UiO-66(NH$_2$) had lower q_{max} values than did MOF-808, possibly due to the blockage of their narrow pores by GLY, which prevents them from accessing Zr sites. This indicates that increasing the linker topicity and consequently forming larger pores

Table 7 Commercial value of typical ligands for ZrMOFs, quoted in 2023

MOF	Linker	CAS	Value ($) (100 g)
NU-1000	4,4',4'',4'''-(Pyrene-1,3,6,8- tetrayl) tetrabenzoic	933047-52-0	28,722,00
UiO-67	4,4'-biphenyldicarboxylic acid	787-70-2	2708,00
UiO-66(NH$_2$)	2-aminoterephthalic acid	10312-55-7	582,00
MOF-808	benzene-1,3,5-tricarboxylic acid	554-95-0	90,00
UiO-66	terephthalic acid	100-21-0	57,00

is a strategy to improve the adsorption performance of MOFs with the same SBU, avoiding the use of longer and more expensive linkers. As expected, the presence of the amino group in UiO-66(NH$_2$) did not influence the adsorption of GLY in the UiO-66 series, indicating that hydrogen bonding interactions are not the main interactions between GLY and the ZrMOFs in this work.

Declarations

Ethical statement The authors declare that ethical approval does not apply to this work because humans and/or animals did not participate in the research.

Competing interests The authors declare no competing interests.

References

1. Ahmadijokani, F., Molavi, H., Rezakazemi, M., Li, J., Arjmand, M.: Progress in materials science UiO-66 metal – organic frameworks in water treatment: a critical review. Prog. Mater. Sci. **125**, 100904 (2022)
2. Al-Ghouti, M.A., Da'ana, D.A.: Guidelines for the use and interpretation of adsorption isotherm models: A review. J. Hazard. Mater. **393**, 122383 (2020). https://doi.org/10.1016/j.jhazmat.2020.122383
3. Alves Monteiro da Silva, D., Alves Monteiro da Silva, S., Trigueiro da Silva, S., de Melo Félix, H.R., Ferraro de Andrade Pessoa, G.G., Eraldo Souza Araújo, J.R., Barbosa da Silva, J.H., Less-aBulhões, L.E., de Oliveira Santos, J.P.: Riscos para a saúde do trabalhador e boas práticas de segurança do trabalho na aplicação de herbicidas em cana-de-açúcar. Sist. Gestão **17**, 80–88 (2022). https://doi.org/10.20985/1980-5160.2022.v17n1.1784
4. de Amarante Junior, O.P., dos Santos, T.C.R., Brito, N.M., Ribeiro, M.L.: Glifosato: propriedades, toxicidade, usos e legislação. Quim. Nova **25**, 589–593 (2002). https://doi.org/10.1590/s0100-40422002000400014
5. Ardila-Suárez, C., Díaz-Lasprilla, A.M., Díaz-Vaca, L.A., Balbuena, P.B., Baldovino-Medrano, V.G., Ramírez-Caballero, G.E.: Synthesis, characterization, and postsynthetic modification of a micro/mesoporous zirconium-tricarboxylate metal-organic framework: towards the addition of acid active sites. CrystEngComm **21**, 3014–3030 (2019). https://doi.org/10.1039/c9ce00218a
6. Batten, S.R., Champness, N.R., Chen, X.M., Garcia-Martinez, J., Kitagawa, S., Öhrström, L., O'Keeffe, M., Suh, M.P., Reedijk, J.: Terminology of metal-organic frameworks and coordination polymers (IUPAC recommendations 2013). Pure Appl. Chem. **85**, 1715–1724 (2013). https://doi.org/10.1351/PAC-REC-12-11-20
7. Bose, S., Senthil Kumar, P., Rangasamy, G., Prasannamedha, G., Kanmani, S.: A review on the applicability of adsorption techniques for remediation of recalcitrant pesticides. Chemosphere **313**, 137481 (2023). https://doi.org/10.1016/j.chemosphere.2022.137481
8. Cavka, J.H., Jakobsen, S., Olsbye, U., Guillou, N., Lamberti, C., Bordiga, S., Lillerud, K.P.: A new zirconium inorganic building brick forming metal organic frameworks with exceptional stability. J. Am. Chem. Soc. **130**, 13850–13851 (2008). https://doi.org/10.1021/ja8057953
9. Chavan, S.M., Shearer, G.C., Svelle, S., Olsbye, U., Bonino, F., Ethiraj, J., Lillerud, K.P., Bordiga, S.: Synthesis and characterization of amine-functionalized mixed-ligand metal-organic frameworks of UiO-66 topology. Inorg. Chem. **53**, 9509–9515 (2014). https://doi.org/10.1021/ic500607a
10. Connolly, A., Leahy, M., Jones, K., Kenny, L., Coggins, M.A.: Glyphosate in Irish adults - a pilot study in 2017. Environ. Res. **165**, 235–236 (2018). https://doi.org/10.1016/j.envres.2018.04.025
11. Coutinho, C.F.B., Mazo, L.H.: Complexos metálicos com o herbicida glifosato: revisão. Quim. Nova **28**, 1038–1045 (2005)
12. DemirDuman, F., Monaco, A., Foulkes, R., Becer, C.R., Forgan, R.S.: Glycopolymer-functionalized MOF-808 nanoparticles as a Cancer-targeted dual drug delivery system for carboplatin and Floxuridine. ACS Appl. Nano Mater. **5**, 13862–13873 (2022). https://doi.org/10.1021/acsanm.2c01632
13. Diercks, C.S., Kalmutzki, M.J., Diercks, N.J., Yaghi, O.M.: Conceptual advances from Werner complexes to metal-organic frameworks. ACS Cent. Sci. **4**, 1457–1464 (2018). https://doi.org/10.1021/acscentsci.8b00677
14. Drout, R.J., Kato, S., Chen, H., Son, F.A., Otake, K.I., Islamoglu, T., Snurr, R.Q., Farha, O.K.: Isothermal titration calorimetry to

explore the parameter space of organophosphorus agrochemical adsorption in MOFs. J. Am. Chem. Soc. **142**, 12357–12366 (2020). https://doi.org/10.1021/jacs.0c04668

15. Ejsmont, A., Andreo, J., Lanza, A., Galarda, A., Macreadie, L., Wuttke, S., Canossa, S., Ploetz, E., Goscianska, J.: Applications of reticular diversity in metal–organic frameworks: An ever-evolving state of the art. Coord. Chem. Rev. **430**, 213655 (2021). https://doi.org/10.1016/j.ccr.2020.213655

16. Fang, F., Lv, Q., Li, P., Tao, Y., Zhang, Y., Zhou, Y., Li, X., Li, J.: Screening of hierarchical porous UiO-67 for efficient removal of glyphosate from aqueous solution. J. Environ. Chem. Eng. **10**, 107824 (2022). https://doi.org/10.1016/j.jece.2022.107824

17. Feng, D., Xia, Y.: Comparisons of glyphosate adsorption properties of different functional Cr-based metal–organic frameworks. J. Sep. Sci. **41**, 732–739 (2018). https://doi.org/10.1002/jssc.201700886

18. Feng, L., Yuan, S., Zhang, L.L., Tan, K., Li, J.L., Kirchon, A., Liu, L.M., Zhang, P., Han, Y., Chabal, Y.J., Zhou, H.C.: Creating hierarchical pores by controlled linker thermolysis in multivariate metal-organic frameworks. J. Am. Chem. Soc. **140**, 2363–2372 (2018). https://doi.org/10.1021/jacs.7b12916

19. Furukawa, H., Cordova, K.E., O'Keeffe, M., Yaghi, O.M.: The chemistry and applications of metal-organic frameworks. Science (80-) **341**, 1230444 (2013). https://doi.org/10.1126/science.1230444

20. Furukawa, H., Gándara, F., Zhang, Y.B., Jiang, J., Queen, W.L., Hudson, M.R., Yaghi, O.M.: Water adsorption in porous metal-organic frameworks and related materials. J. Am. Chem. Soc. **136**, 4369–4381 (2014). https://doi.org/10.1021/ja500330a

21. Galaço, A.R.B.S., Jesus, L.T., Freire, R.O., De Oliveira, M., Serra, O.A.: Experimental and theoretical studies of glyphosate detection in water by an europium luminescent complex and effective adsorption by HKUST-1 and IRMOF-3. J. Agric. Food Chem. **68**, 9664–9672 (2020). https://doi.org/10.1021/acs.jafc.0c03574

22. HormoziJangi, S.R., Akhond, M.: High throughput urease immobilization onto a new metal-organic framework called nanosized electroactive quasi-coral-340 (NEQC-340) for water treatment and safe blood cleaning. Process Biochem. **105**, 79–90 (2021). https://doi.org/10.1016/j.procbio.2021.03.027

23. Huang, L., Shen, R., Shuai, Q.: Adsorptive removal of pharmaceuticals from water using metal-organic frameworks: A review. J. Environ. Manage. **277**, 111389 (2021). https://doi.org/10.1016/j.jenvman.2020.111389

24. Iwuozor, K.O., Emenike, E.C., Gbadamosi, F.A., Ighalo, J.O., Umenweke, G.C., Iwuchukwu, F.U., Nwakire, C.O., Igwegbe, C.A.: Adsorption of organophosphate pesticides from aqueous solution: a review of recent advances. Springer, Berlin Heidelberg (2022)

25. Jia, D., Guo, J., Li, J., Duan, Y.: Removal of glyphosate from aqueous solution by CuO coated MIL-101(Fe). Can. J. Chem. Eng. **101**, 1–11 (2022). https://doi.org/10.1002/cjce.24702

26. Kadhom, M., Deng, B.: Metal-organic frameworks (MOFs) in water filtration membranes for desalination and other applications. Appl. Mater. Today **11**, 219–230 (2018). https://doi.org/10.1016/j.apmt.2018.02.008

27. Kalmutzki, M.J., Hanikel, N., Yaghi, O.M.: Secondary building units as the turning point in the development of the reticular chemistry of MOFs. Sci. Adv. **4**, eaat9180 (2018). https://doi.org/10.1126/sciadv.aat9180

28. Kandiah, M., Nilsen, M.H., Usseglio, S., Jakobsen, S., Olsbye, U., Tilset, M., Larabi, C., Quadrelli, E.A., Bonino, F., Lillerud, K.P.: Synthesis and stability of tagged UiO-66 Zr-MOFs. Chem. Mater. **22**, 6632–6640 (2010). https://doi.org/10.1021/cm102601v

29. Kirlikovali, K.O., Hanna, S.L., Son, F.A., Farha, O.K.: Back to the basics: developing advanced metal-organic frameworks using fundamental chemistry concepts. ACS Nanosci. Au (2022). https://doi.org/10.1021/acsnanoscienceau.2c00046

30. Liu, R., Xie, Y., Cui, K., Xie, J., Zhang, Y., Huang, Y.: Adsorption behavior and adsorption mechanism of glyphosate in water by amino-MIL-101(Fe). J. Phys. Chem. Solids **161**, 110403 (2022). https://doi.org/10.1016/j.jpcs.2021.110403

31. Liu, X., Kirlikovali, K.O., Chen, Z., Ma, K., Idrees, K.B., Cao, R., Zhang, X., Islamoglu, T., Liu, Y., Farha, O.K.: Small molecules, big effects: tuning adsorption and catalytic properties of metal-organic frameworks. Chem. Mater. **33**, 1444–1454 (2021). https://doi.org/10.1021/acs.chemmater.0c04675

32. Logan, M.W., Langevin, S., Xia, Z.: Reversible atmospheric water harvesting using metal-organic frameworks. Sci. Rep. **10**, 1–11 (2020). https://doi.org/10.1038/s41598-020-58405-9

33. Mali, H., Shah, C., Raghunandan, B.H., Prajapati, A.S., Patel, D.H., Trivedi, U., Subramanian, R.B.: Organophosphate pesticides an emerging environmental contaminant: pollution, toxicity, bioremediation progress, and remaining challenges. J. Environ. Sci. **127**, 234–250 (2022). https://doi.org/10.1016/j.jes.2022.04.023

34. Manogaran, M., Shukor, M.Y., Yasid, N.A., Johari, W.L.W., Ahmad, S.A.: Isolation and characterization of glyphosate-degrading bacteria isolated from local soils in Malaysia. Rend. Lincei **28**, 471–479 (2017). https://doi.org/10.1007/s12210-017-0620-4

35. Molavi, H., Eskandari, A., Shojaei, A., Mousavi, S.A.: Enhancing CO2/N2 adsorption selectivity via post-synthetic modification of NH2-UiO-66(Zr). Microporous Mesoporous Mater. **257**, 193–201 (2018). https://doi.org/10.1016/j.micromeso.2017.08.043

36. Naghdi, S., Brown, E., Zendehbad, M., Duong, A., Ipsmiller, W., Biswas, S., Toroker, M.C., Kazemian, H., Eder, D.: Glyphosate adsorption from water using hierarchically porous metal-organic frameworks. Adv. Funct. Mater. **33**, 2213862 (2023). https://doi.org/10.1002/adfm.202213862

37. Nargis, F., Duong, A., Rehl, E., Bradshaw, C., Kazemian, H.: Highly efficient and low-cost clay-based adsorbent for glyphosate removal from contaminated water. Chem. Eng. Technol. **45**, 340–347 (2022). https://doi.org/10.1002/ceat.202100437

38. Pankajakshan, A., Sinha, M., Ojha, A.A., Mandal, S.: Water-stable nanoscale zirconium-based metal-organic frameworks for the effective removal of glyphosate from aqueous media. ACS Omega **3**, 7832–7839 (2018). https://doi.org/10.1021/acsomega.8b00921

39. Pereira, H.A., Hernandes, P.R.T., Netto, M.S., Reske, G.D., Vieceli, V., Oliveira, L.F.S., Dotto, G.L.: Adsorbents for glyphosate removal in contaminated waters: a review. Environ. Chem. Lett. **19**, 1525–1543 (2021). https://doi.org/10.1007/s10311-020-01108-4

40. Reinsch, H., Waitschat, S., Chavan, S.M., Lillerud, K.P., Stock, N.: A Facile, "Green" route for scalable batch production and continuous synthesis of zirconium MOFs. Eur. J. Inorg. Chem. **2016**, 4490–4498 (2016). https://doi.org/10.1002/ejic.201600295

41. Rivas-Garcia, T., Espinosa-Calderón, A., Hernández-Vázquez, B., Schwentesius-Rindermann, R.: Overview of environmental and health effects related to glyphosate usage. Sustainability **14**, 6868 (2022). https://doi.org/10.3390/su14116868

42. Tao, Y., Fang, F., Lv, Q., Qin, W., He, X., Zhang, Y., Zhou, Y., Li, X., Li, J.: Highly efficient removal of glyphosate from water by hierarchical-pore UiO-66: Selectivity and effects of natural water particles. J. Environ. Manage. **316**, 115301 (2022). https://doi.org/10.1016/j.jenvman.2022.115301

43. Tran, H.N., You, S.J., Hosseini-Bandegharaei, A., Chao, H.P.: Mistakes and inconsistencies regarding adsorption of contaminants from aqueous solutions: a critical review. Water Res. **120**, 88–116 (2017). https://doi.org/10.1016/j.watres.2017.04.014

44. Tranchemontagne, D.J., Hunt, J.R., Yaghi, O.M.: Room temperature synthesis of metal-organic frameworks: MOF-5, MOF-74,

MOF-177, MOF-199, and IRMOF-0. Tetrahedron **64**, 8553–8557 (2008). https://doi.org/10.1016/j.tet.2008.06.036

45. Valenzano, L., Civalleri, B., Chavan, S., Bordiga, S., Nilsen, M.H., Jakobsen, S., Lillerud, K.P., Lamberti, C.: Disclosing the complex structure of UiO-66 metal organic framework: a synergic combination of experiment and theory. Chem. Mater. **23**, 1700–1718 (2011). https://doi.org/10.1021/cm1022882

46. Van Bruggen, A.H.C., He, M.M., Shin, K., Mai, V., Jeong, K.C., Finckh, M.R., Morris, J.G.: Environmental and health effects of the herbicide glyphosate. Sci. Total. Environ. **616–617**, 255–268 (2018). https://doi.org/10.1016/j.scitotenv.2017.10.309

47. Wang, J., Guo, X.: Adsorption kinetic models: physical meanings, applications, and solving methods. J. Hazard. Mater. **390**, 122156 (2020). https://doi.org/10.1016/j.jhazmat.2020.122156

48. Wang, Q., Cui, K.P., Liu, T., Li, C.X., Liu, J., Kong, D.C., Weerasooriya, R., Chen, X.: In situ growth of NH2-MIL-101 metal organic frameworks on biochar for glyphosate adsorption. Chemosphere. **331**, 138827 (2023). https://doi.org/10.1016/j.chemosphere.2023.138827

49. Wen, Y., Feng, M., Zhang, P., Zhou, H.-C., Sharma, V.K., Ma, X.: Metal Organic Frameworks (MOFs) as photocatalysts for the degradation of agricultural pollutants in water. ACS ES&T Eng. **1**, 804–826 (2021). https://doi.org/10.1021/acsestengg.1c00051

50. Baldi, I., Blair, A., Calaf, G.M., Egeghy, P.P., Forastiere, F., Fritschi, L., Jahnke, G.D., Jameson, C.W., Kromhout, H., Curieux, F. Le., Martin, M.T., McLaughlin, J., Rodriguez, T., Ross, M.K., Rusyn, I.I., Sergi, C.M., Mannetje, A., Zeise, L.: Glyphosate. In: Some organophosphate insecticides and herbicides/ IARC Working Group on the Evaluation of Carcinogenic Risks to Humans, pp 321–399. Iarc Monographs. V.112, Switzerland (2015)

51. Williams, G.M., Aardema, M., Acquavella, J., Berry, S.C., Brusick, D., Burns, M.M., de Camargo, J.L.V., Garabrant, D., Greim, H.A., Kier, L.D., Kirkland, D.J., Marsh, G., Solomon, K.R., Sorahan, T., Roberts, A., Weed, D.L.: A review of the carcinogenic potential of glyphosate by four independent expert panels and comparison to the IARC assessment. Crit. Rev. Toxicol. **46**, 3–20 (2016). https://doi.org/10.1080/10408444.2016.1214677

52. Xu, J., Liu, J., Li, Z., Wang, X., Xu, Y., Chen, S., Wang, Z.: Optimized synthesis of Zr(iv) metal organic frameworks (MOFs-808) for efficient hydrogen storage. New J. Chem. **43**, 4092–4099 (2019). https://doi.org/10.1039/C8NJ06362A

53. Yaghi, O.M., Kalmutzki M.J., Diercks, C.S.: Introduction to Reticular Chemistry. Wiley – VCH, Weinheim (2019)

54. Yang, Q., Wang, J., Zhang, W., Liu, F., Yue, X., Liu, Y., Yang, M., Li, Z., Wang, J.: Interface engineering of metal organic framework on graphene oxide with enhanced adsorption capacity for organophosphorus pesticide. Chem. Eng. J. **313**, 19–26 (2017). https://doi.org/10.1016/j.cej.2016.12.041

55. Yang, Q., Wang, J., Chen, X., Yang, W., Pei, H., Hu, N., Li, Z., Suo, Y., Li, T., Wang, J.: The simultaneous detection and removal of organophosphorus pesticides by a novel Zr-MOF based smart adsorbent. J. Mater. Chem. A. **6**, 2184–2192 (2018). https://doi.org/10.1039/c7ta08399h

56. Yang, X., Li, Z., Tang, S.: Tailored design of hierarchically porous UiO-66 with a controlled pore structure and metal sites. Cryst. Growth Des. **21**, 6092–6100 (2021). https://doi.org/10.1021/acs.cgd.1c00411

57. Zhu, X., Li, B., Yang, J., Li, Y., Zhao, W., Shi, J., Gu, J.: Effective adsorption and enhanced removal of organophosphorus pesticides from aqueous solution by Zr-Based MOFs of UiO-67. ACS Appl. Mater. Interfaces **7**, 223–231 (2015). https://doi.org/10.1021/am5059074